THE JOURNAL OF PHYSICAL CHEMISTRY C
A JOURNAL OF THE AMERICAN CHEMICAL SOCIETY

pubs.acs.org/JPCC

Article

Synthesis of Atomically Dispersed Rh Catalysts on Oxide Supports via Strong Electrostatic Adsorption and Characterization by Cryogenic Infrared Spectroscopy

Chithra Asokan, Mingjie Xu, Sheng Dai, Xiaoqing Pan, and Phillip Christopher*

Cite This: *J. Phys. Chem. C* 2022, 126, 18704–18715

Read Online

ACCESS | Metrics & More | Article Recommendations | Supporting Information

ABSTRACT: Oxide-supported Rh catalysts are utilized in applications ranging from NO_x reduction reactions in automotive catalysis to hydrogenation reactions in hydrocarbon upgrading. Interest in synthesizing catalysts in which Rh exists as atomically dispersed species on oxide supports rather than Rh nanoparticles derives from the potential to promote the efficient use of this rare element and uncover alternative catalytic reactivity. Synthesizing atomically dispersed Rh catalysts is challenging because the metal species often thermodynamically prefer to form clusters. Characterizing the structure of oxide-supported Rh species can also be challenging because Rh is known to be mobile on oxide supports, leading to sintering or redispersion during characterization. Here, we establish the influence of pH, Rh precursor speciation, and support composition on the synthesis of atomically dispersed Rh species on commercially relevant oxide supports (CeO_2 and γ-Al_2O_3) via strong electrostatic adsorption. CO probe molecule infrared spectroscopy (CO-FTIR) is used to distinguish atomically dispersed Rh species from Rh clusters, and focus is placed on measurements at cryogenic temperature that prevent Rh mobility. The structural analysis of Rh species by CO-FTIR is substantiated by aberration-corrected scanning transmission electron microscopy imaging. It is observed that synthesis conditions that are optimum for strong electrostatic adsorption of Rh precursors onto the oxide supports are also optimum for producing atomically dispersed Rh species. The synthesis and characterization approach presented here provides a methodology that could facilitate the development of structure–function relationships for catalytic reactions.

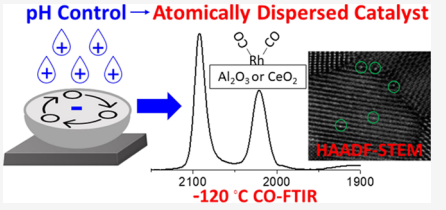

1. INTRODUCTION

Atomically dispersed metal catalysts have the potential to provide optimal utilization of expensive precious metals and distinct reactivity compared to metal clusters. Atomically dispersed metal active sites are likely present in many industrial catalysts, particularly where low metal weight loadings are commonly used, such as in the three-way catalyst (TWC) in catalytic converters.[1] TWCs contain mixtures of precious metals, such as Pd and Rh, that catalyze the conversion of species present in the exhaust of gasoline burning engines, such as NO_x and carbonaceous byproducts, into nontoxic gases.[2−4] TWCs commonly contain less than 0.5% Rh, which exists as a mixture of large particles, small clusters, and atomically dispersed species.[5] While much work has been dedicated to studying the reactivity of Rh nanoparticles and extended surfaces for NO_x reduction reactions, there exist minimal insights into the role of atomically dispersed Rh species in automotive catalysis.[6−14]

Interrogating the reactivity of atomically dispersed Rh active sites is challenging due to difficulties with the synthesis of catalysts that contain exclusively these species, the stability of these species under reaction environments, and characterization of the distribution of active site structures.[15] Recently, stable catalysts consisting of atomically dispersed Pt species on TiO_2 and CeO_2 were synthesized by applying principles of strong electrostatic adsorption (SEA), using low Pt weight loadings, and employing small-diameter (∼5 nm) oxide nanoparticles as supports.[16−20] Using small oxide nanoparticles as supports minimizes potential interactions between atomically dispersed metal species on the support due to the low number of metal species that exist on each particle.[18,21] This approach has enabled the synthesis of catalysts containing predominantly atomically dispersed metal species and stability against sintering, even in reducing environments.

While SEA has been demonstrated as effective for synthesizing highly dispersed Pt catalysts, few works exist on using SEA for the synthesis of highly dispersed Rh catalysts.[22−29] An important distinction between SEA-based synthesis of Pt and Rh catalysts is the speciation of common precursors under pH-controlled aqueous environments.[30] For the case of Pt, widely available and commonly used precursors such as H_2PtCl_6 and $Pt(NH_4)_4(NO_3)_2$ form distinct and stable ions in pH-controlled aqueous solutions, making it relatively

Received: August 1, 2022
Revised: October 10, 2022
Published: October 27, 2022

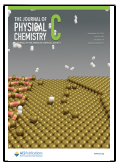

https://doi.org/10.1021/acs.jpcc.2c05426
J. Phys. Chem. C 2022, 126, 18704−18715

straightforward to predict the interaction between metal precursors and charged oxide support surfaces. Alternatively, common Rh precursors, such as $RhCl_3$ and $Rh(NO_3)_3$, speciate to form a distribution of ions in solution as a function of pH.[31,32] The variation of Rh ions present in solution makes it challenging to identify synthetic conditions that maximize metal dispersion as electrostatic interactions in solution between metal precursors and support surfaces are key to SEA syntheses.[22,23,25,27,33−36]

There are also challenges associated with characterizing the distribution of Rh structures in a synthesized catalyst. For example, imaging of Rh structure distribution down to the limit of single atoms by scanning transmission electron microscopy (STEM) is challenging for supports containing heavy cations (e.g., CeO_2) because of the lack of Z-contrast between Rh and Ce.[37−39] Furthermore, X-ray absorption spectroscopy provides only a measure of the average coordination environment of Rh species, rather than information about the distribution of Rh structures. CO probe molecule Fourier-transform infrared spectroscopy (CO-FTIR) is a powerful technique for characterizing the distribution of Rh species in a catalyst sample.[40−48] This stems from the distinct bonding geometry of CO to Rh clusters and atomically dispersed Rh species and the known site-specific extinction coefficients for the resulting CO stretches.[49−52] Although using CO as a probe molecule can be informative, CO can oxidatively fragment Rh clusters into atomically dispersed Rh species. Fragmentation occurs under CO environments because of the thermodynamic preference of Rh to exist as atomically dispersed gem dicarbonyl species, $Rh(CO)_2$, on the oxide support rather than CO-saturated Rh clusters.[53−56] Notably, gem dinitrosyl, $Rh(NO)_2$, formation and identification by FTIR has also been reported as a characterization method for atomically dispersed Rh species in zeolites. However, unlike atomically dispersed Rh species in zeolites, NO probe molecule FTIR spectra for atomically dispersed Rh on Al_2O_3 and CeO_2 show no observable $Rh(NO)_x$ signatures at ambient and higher temperatures.[57] The absence of bands associated with $Rh(NO)_x$ on these oxide supports at ambient or higher temperatures indicates that once NO adsorbs to Rh, it rapidly reacts to form N_2O, NO_2, or N_2.

In this work, we analyze how the conditions (Rh weight loading and solution pH) of SEA-based synthesis of Rh catalysts on Al_2O_3 and CeO_2 supports, the most common supports in TWC, influence the resulting distribution of Rh species. The electrostatic adsorption of Rh precursors onto the oxide supports was experimentally and theoretically analyzed by considering the pH-dependent speciation of $RhCl_3$ in solution and the interactions of these species with the oxide surfaces.[30] Cryogenic probe molecule CO-FTIR was used to characterize the distribution of Rh structures, and low-temperature analysis was shown to be critical to minimize CO-induced fragmentation of Rh clusters that is prevalent at room temperature. FTIR-based characterization was supported with high-angle annular dark-field STEM (HAADF-STEM) to substantiate conclusions regarding the Rh structure.[19,20,48,58] We identify simple synthetic protocols and characterization approaches for the production and characterization of atomically dispersed Rh species on CeO_2 and Al_2O_3. We expect that model catalysts synthesized through this approach will help rationalize the performance of industrial Rh catalysts and provide design rules for enhanced catalyst performance.

2. MATERIALS AND METHODS

2.1. Materials. Rhodium(III) chloride hydrate ($RhCl_3 \cdot xH_2O$) purchased from Sigma-Aldrich (#206261) was used as a precursor for catalyst synthesis. High-surface-area CeO_2 (70 m^2/g) and γ-Al_2O_3 (127 m^2/g) nanoparticles (5−10 nm diameter) were purchased from US Research Nanomaterials (US Nano Stock #US3037 and #US3007, respectively). Reagent grade ammonium hydroxide, NH_4OH, (28−30% concentration obtained from Sigma-Aldrich, #221228) was used to produce basic pH solutions. Diluted hydrochloric acid, HCl, (certified ACS Plus 36.5 to 38.0% from Fisher Chemical) was used to produce acidic pH solutions. High-performance liquid chromatography (HPLC) grade water from J.T Baker (#4218) was used for all dilutions.

2.2. Point of Zero Net Charge Measurements. The point of zero net charge (PZNC) was experimentally determined by titration of the oxide supports with protons from solution. A series of eight 30 mL aqueous solutions with acidic or basic pH values (~1, 2, 3, 4, 5, 8, 9, 10, and 11) were prepared through the addition of diluted HCl or NH_4OH. Dry oxide powder (20 mg) was added to each solution and thoroughly mixed for 1 h. The pH of the equilibrated solutions was measured, and the PZNC was determined by averaging final pH values at the plateau where the support reaches a neutral charge due to proton exchange (Figure S1).

2.3. Analysis of Rh Precursor Speciation. To measure the speciation of $RhCl_3$ in solution, UV−vis spectroscopy (via a Thermo Scientific Evolution 300 spectrophotometer) and electrospray ionization-mass spectrometry, ESI-MS, (via Waters LCT Premier ESI TOF with a high-resolution orthogonal Time-of-Flight mass spectrometer operating in the 100−2000 m/z range and multimode ionization source for fast switching between positive and negative polarities) were used. $RhCl_3 \cdot xH2O$ was diluted in water to make a 60 mL stock solution containing 125 ppm of Rh. The stock solution was split into six solutions. One solution was kept aside without adjustment, which stabilized at a pH of ~3. The remaining solutions were adjusted with NH_4OH to target pH values 5, 8, 9, 10, and 11 within +/−0.5 to be analyzed by ESI-MS and UV−vis.

2.4. Rhodium Uptake Measurements. The uptake of Rh onto the oxide supports was determined by mixing pH-adjusted oxide and precursor solutions, followed by filtration to retrieve the oxide support and analysis of the residual Rh concentration in solution by inductively coupled plasma optical emission spectroscopy, ICP-OES (Thermo iCAP 6300). The ICP-OES measurements were calibrated using stock Rh solutions (0−500 ppm) made from diluting a commercial Rh standard (Millipore #04736) with 2% HCl. A series of solutions containing 50 mg of oxide support with final pH values of 3, 5, 8, 9, 10, and 11 and corresponding pH-adjusted solutions containing 200 ppm of $RhCl_3 \cdot xH_2O$ were prepared using NH_4OH or HCl. The liquid ratio of the precursor to support solution was 1:5, which resulted in nominal 2 wt % Rh on the oxide support if all Rh adsorbed. Support solutions were mixed with their corresponding precursor solutions with the same pH for 1 h. The solute was filtered under vacuum with a Lab Safety Supply Filter Paper (#14A842, pore 0.45 μm, 4.7 cm diameter), and the filtrate was kept for analysis. The percent uptake of the Rh precursor by the oxide support was calculated by subtracting the final Rh concentration from the initial concentration

https://doi.org/10.1021/acs.jpcc.2c05426
J. Phys. Chem. C 2022, 126, 18704−18715

measured by ICP-OES. Each experiment was repeated three times, and the reported values are the average and standard deviation of the triplicate experiments.

2.5. Rh Deposition at Various Weight Loadings. 100 mg of CeO_2 or γ-Al_2O_3 support and the desired amount of the $RhCl_3$ precursor based on the targeted wt % were diluted in water separately to create separate solutions at a volumetric ratio of 4:1 (support liquid solution: precursor liquid solution) to combine for a total of 100 mL. Diluted NH_4OH or HCl was added to the support and precursor solutions to target pH values corresponding to those used in the Rh uptake analyses. The precursor solution was injected by a 30 mL glass syringe with a stainless-steel needle using a programmable single channel infusion pump at a rate of 4 mL/min into the support solution while constantly stirring. Then, the solution was heated to 70 °C while being mixed in an evaporation dish until water was evaporated, and the sample was dried completely (approximately 2.5 h). The sample was then kept overnight at 100 °C in an oven and then ex situ calcined in dry air for 4 h at 350 °C.

2.6. Cryogenic IR Characterization. Materials were loaded into a Harrick low-temperature reaction chamber mounted inside a ThermoScientific Praying Mantis diffuse reflectance adapter. A Nicolet iS10 FTIR spectrometer with a Mercury Cadmium Telluride (MCT) detector cooled by liquid nitrogen was used to collect IR spectra. All gases were passed across an isopropyl alcohol-liquid nitrogen cold trap held at −40 °C and a glass trap filled with the Drierite desiccant to remove trace moisture. Materials were pretreated in situ by oxidation for 30 min at 350 °C in pure O_2, followed by reduction for 1 h at 200 °C in 10% H_2/Ar. In situ oxidation was used to remove residual moisture or organics deposited on the material upon exposure to the atmosphere while being stored, while the 4 h calcination in air following initial synthesis was used to remove precursor ligands and remaining chemical residues such as excess NH_4OH. The subsequent reduction treatment reduced Rh to a lower oxidation state and enabled CO adsorption. Following pretreatment, materials were cooled to cryogenic temperatures (−120 °C) in Ar under vacuum and then exposed to 10% CO/Ar for 10 min, followed by purging in Ar for 10 min. Spectra were recorded with 32 scans and 0.482 cm^{-1} data spacing. To track Rh structure changes as temperature was increased to room temperature, spectra were continuously collected, while 10% CO/Ar was flown in vacuum. In all measurements, spectra were obtained by averaging 32 sequentially collected scans at a resolution of 4 cm^{-1} in absorbance mode.

2.7. Scanning Transmission Electron Microscopy. Samples were oxidized ex situ at 350 °C for 30 min in pure O_2 and then reduced at 200 °C for 60 min in 10% H_2/He. HAADF-STEM images were taken on a JEOL Grand ARM 300CF TEM/STEM with double spherical aberration correctors operated at 300 kV with a probe current of 23 pA and a pixel time of 4 μs. Samples for STEM measurements were prepared by dropping 60 μL of the catalyst dispersed in methanol on a lacey carbon-coated copper grid.

3. RESULTS

3.1. pH-Dependent Oxide Surface Charge and Rh Precursor Speciation. We were motivated to study SEA as a mechanism for the synthesis of atomically dispersed metal catalysts due to the scalability and industrial viability of the method.[22,34,35] The fundamental concept relies on the electrostatic adsorption of ligated metal ions from solution onto specific surface sites on the support.[24,25,27] At low metal loadings, the synthesis approach produces isolated metal ion precursors well distributed on the support. Thus, if electrostatic interactions between metal precursors and support surfaces are well-designed and pretreatment steps are chosen to minimize metal mobility, a facile and scalable synthetic method for atomically dispersed metal catalysts can be realized.

Hydroxyls on oxide surfaces play a central role in SEA-based syntheses as their local environments and proton exchange with solution dictate the local oxide surface charge. Hydroxyls at the surface of metal oxides compensate for charge deficiency in the oxide.[59] Hydroxyl species can exhibit a uniform distribution of charge density across an oxide surface, or more often, hydroxyls exhibit varying charge densities across the support due to defects in the oxide structure and the exposure of distinct oxide facets.[60] The nature of hydroxyls on an oxide surface and relative abilities to protonate or deprotonate dictate the pH conditions where energetically favorable electrostatic interactions exist with metal ion precursors in solution.[56,61]

When an oxide surface is in contact with a solution containing ions, charged species will adsorb or desorb from the surface to equilibrate with the surroundings. Under certain conditions, equilibration of an oxide surface with an aqueous environment will result in a neutral oxide surface charge. The pH of the solution where the oxide surface becomes neutral is known as the PZNC.[24,62] The PZNC can result from a homogeneously neutral surface or a surface where there is an even but heterogeneous distribution of positive and negative charges. The electrostatic adsorption of Rh ions onto an oxide surface requires the existence of pH where the metal ion charge in solution is opposite to that of the net charge of the support surface. This results in a negative Gibbs free energy associated with the electrostatic interaction between the metal ion and the oxide surface and thus electrostatic adsorption. CeO_2 and γ-Al_2O_3, the most prevalent supports in TWC and the focus of this study, exhibit distinct hydroxyl characteristics across their surfaces and therefore should require different optimal solution pHs for the SEA-based synthesis of atomically dispersed Rh catalysts.

We start by considering the pH-dependent charge of the oxide support surfaces. The PZNCs for small CeO_2 and γ-Al_2O_3 nanoparticles were estimated by measuring the uptake and removal of protons from the oxide surfaces, Figure S1. The PZNC values for CeO_2 and γ-Al_2O_3 were measured as 3.3 and 7.2, respectively, which are consistent with previous literature reports.[24] Because γ-Al_2O_3 has a PZNC at near neutral pH, cationic or anionic Rh precursors should electrostatically adsorb by working at basic or acidic synthesis pH, respectively. Alternatively, CeO_2 has a large pH range (above the PZNC) where favorable interactions with cationic Rh precursors exist but only a minimal pH window where adsorption of anionic Rh precursors would be favorable.[63] Thus, CeO_2 should be able to electrostatically adsorb Rh cations when the solution pH is greater than 3.3. γ-Al_2O_3 should adsorb Rh cations when the solution pH is greater than 7.2 or absorb Rh anions when the solution pH is lower than 7.2. However, the uptake of metal ions onto oxide surfaces typically occurs well above or below the PZNC once the strength of the electrostatic attraction is sufficiently large.

A key component and complication to the SEA-based synthesis of supported Rh catalysts is the speciation of Rh ions

https://doi.org/10.1021/acs.jpcc.2c05426
J. Phys. Chem. C 2022, 126, 18704−18715

from common Rh precursors as a function of the pH and composition of the aqueous environment. For example, diluting $RhCl_3{\cdot}xH_2O$ in liquid produces a range of Rh ions with varying Cl, OH, and H_2O coordination, as well as overall charge, which exhibit distinct UV−vis absorbance spectra.[64−67] UV−vis analysis of a dilute (125 ppm Rh with a resulting pH of 3) solution of $RhCl_3{\cdot}xH_2O$ in water results in a spectrum with broad bands at ∼408 and 518 nm, Figure 1a.

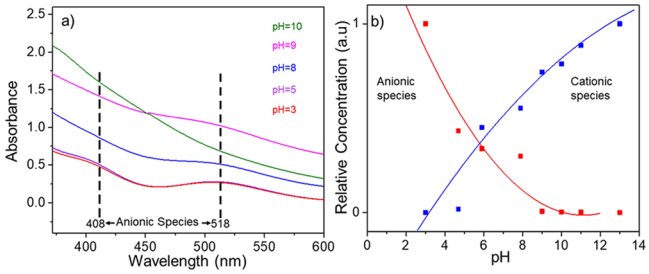

Figure 1. (a) UV−vis spectra of $RhCl_3{\cdot}xH_2O$ diluted in water and with pH adjusted using NH_4OH addition. Features at ∼408 and ∼518 nm assigned to $[Rh(Cl_6)]^{3-}$ or $[RhCl_5(H_2O)]^{2-}$ are noted with vertical dashed lines. (b) Relative concentrations of anionic (red) and cationic (blue) Rh species $RhCl_3{\cdot}xH_2O$ solutions measured by the ESI-MS peak area as a function of solution pH and associated second-order polynomial fits.

Experimental and theoretical analyses have assigned these features to $RhCl_6^{3-}$ or $RhCl_5(H_2O)^{2-}$.[68−70] The $RhCl_6^{3-}$ complex favorably forms in an acidic solution when excess Cl is present but undergoes fast aquation into $RhCl_5(H_2O)^{2-}$.[67,70,71] In this experiment, no additional Cl was added to the solution, which suggests that $RhCl_6^{3-}$ species either form due to excess Cl concentration in the stock solution or from disproportionation of $RhCl_3$ into species with higher and lower Cl coordination as compared to the starting precursor. The speciation of $RhCl_3$ is known to be fast under these conditions and results in a distribution of the charged metal−aquo complexes.[30,64,70,71]

The broadness of the bands observed in the UV−vis spectra here in comparison to previous measurements on well-defined Rh species suggests that the initial precursor solution contains a range of anionic Rh species with varying Cl, H_2O, and OH coordination.[64] As pH of the solution was increased with NH_4OH addition, the absorbance features associated with anionic Rh−Cl aquo complexes shifted to lower wavelengths (higher energy) and became less resolved, and the overall absorbance of the solution increased. This is consistent with the exchange of Cl ligands for H_2O, OH, or NH_3 and likely results in decreasing negative charge or a switch to positive charge for the Rh ions in solution.[69,71,72] These results are consistent with previous examples where $RhCl_3{\cdot}xH_2O$ undergoes hydrolysis when diluted with water and then, when mixing with desired reagents, results in the formation of new ionic complexes in solution.[69−74] Given the broadness of the bands at low pH and the resulting featureless spectra at higher pH, the results suggest that $RhCl_3$ initially speciates into a range of anionic complexes, which then undergo ligand exchange to begin producing predominantly cationic species above a pH of about 7.

To support conclusions from the UV−vis measurements, ESI-MS measurements were performed. ESI-MS allows analysis of the type of ion complexes present in solution and can be performed in negative and positive ion detection modes to screen both anionic and cationic Rh species.[75] While ionic concentrations cannot be determined quantitatively by ESI-MS, the relative concentrations of positive or negative ionic species can be tracked as a function of pH by examining mass to charge (m/z) peak areas as a function of pH (see Figures 1b, S2, and S3). At an initial pH of 3, when $RhCl_3{\cdot}xH_2O$ was diluted in water (125 ppm Rh), anionic species were observed in the ESI mass spectrum with m/z values of 243.0−246.9 in the negative mode. These features could be assigned to $RhCl^{4-}$, $[RhCl_2(H_2O)_2(OH)_2]^-$, and associated ions, likely formed from $RhCl_3$ reacting with residual Cl present in solution during electrospray ionization when high electron voltage is applied (see Figure S2).[76] The ESI-MS identification of a chlorinated Rh species with anionic charge is consistent with the UV−vis results. The $RhCl_6^{3-}$ complex should in principle be present in the solution analyzed by ESI-MS, as seen in UV−vis, but aquation was likely promoted by the high voltage applied during ESI-MS.[76−78] The positive mode ESI-MS analysis of the pH = 3 solution did not indicate any known m/z values associated with Rh complexes, suggesting that no cationic Rh complexes existed.

As the solution pH was increased above 3 through the addition of NH_4OH, the relative area of peaks observed by ESI-MS in the negative detection mode at 243.0−246.9 decreased and new features at 260.1−266 and 278.9−288.9 appeared that can be attributed to the m/z of ions associated with $RhCl_3(H_2O)_2OH^-$ and $RhCl_4(H_2O)^{2-}$, respectively, which is indicative of the pH-influenced aquation.[76−78] Above a pH of 8, there remained no detectable anionic species by analysis of the ESI-MS in a negative mode. The results are consistent with the UV−vis measurements where a loss of features associated with the anionic chlorinated Rh species was observed at a pH of 9. By positive mode ESI-MS, the cationic Rh species were observed to be present above a pH of 5 (Figure S3). This is consistent with the UV−vis measurements, which showed a transition in the spectra above a pH of 5. The primary positive m/z peak values 112.6−114.9 were assigned to $RhCl(H_2O)_4(NH_3)^{2+}$, $RhCl(H_2O)_3(NH_3)_2^{2+}$, or $RhCl(H_2O)_2(NH_3)_3^{2+}$, all which seem reasonable as ligand exchange products at increasing NH_3 concentrations. The growth in relative intensity of the features associated with cationic Rh species as a function of pH, Figure 1b, is consistent with the loss of anionic species observed from the negative mode ESI-MS. It is interesting to note that there is a range from pH of 5 to 9, where the coexistence of cationic and anionic Rh species is observed.

Based on the UV−vis and ESI-MS, $RhCl_3$ speciates in the aqueous solution to form a distribution of anionic Rh−Cl aquo complexes and then undergoes ligand exchange as NH_4OH is added to increase the solution pH. Evidence was provided that there exist a range of Rh species in solution at each pH and that both cationic and anionic Rh species exist in solution at intermediate pH. A more detailed look at the expected or existing mixture of complexes would require thermodynamic modeling including Cl, OH, H_2O, and NH_3 ions accompanied by X-ray absorption spectroscopy, which is outside the scope of these studies. To effectively model the uptake of Rh ions onto the supports, we simplified the picture to assume that the range of cationic species can be described by a representative $Rh(Cl)_x(H_2O)_y(NH_3)_z^{2+}$ complex, while the anionic species can be described by a representative $Rh(Cl)_x(H_2O)_y(OH)_z^{2-}$ complex, and that their relative concentrations vary as

https://doi.org/10.1021/acs.jpcc.2c05426
J. Phys. Chem. C 2022, 126, 18704−18715

measured by the polynomial fits to the ESI-MS data shown in Figure 1b.

3.2. Uptake Analysis. The uptake of Rh species from solution onto the oxide supports was modeled using the revised physical adsorption (RPA) model.[23,62] The uptake of Rh ions was assumed to follow a Langmuir isotherm adsorption (eq S1) in which the equilibrium constant (eq S2) was calculated using the Coulombic Gibbs free energy (eq S3) of adsorption of Rh ions onto each oxide support. The Gibbs free energy takes into the account the most prevalent Rh species' ionic charge identified by UV−vis and ESI-MS (∼ −2 and +2), relative concentration of ions identified by ESI-MS, Faraday's constant, and the electric double layer potential. The relative concentration of anions and cations was calculated at variable pH using polynomial best fits (eqs S4−S5) of the relative ion concentration measured by the normalized ESI-MS ion peak area as a function of pH (shown in Figure 2b). The

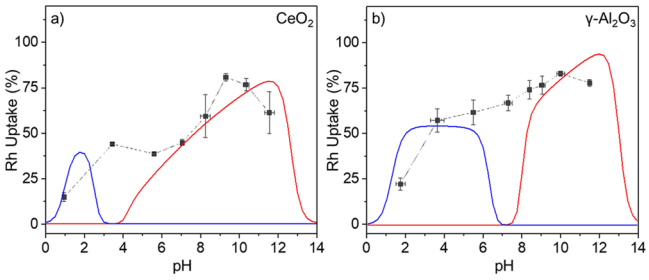

Figure 2. RPA-modeled uptake of Rh anions (blue line) and cations (red line) over a pH range of 0−14 on (a) CeO_2 and (b) γ-Al_2O_3.The experimentally determined %Rh uptake of the 200 ppm Rh solution on 50 mg of oxide support using ICP analysis of pH-adjusted $RhCl_3 \cdot xH_2O$ is shown using black dots. Uptake % is presented as the average of triplicate experiments with error bars representing the standard deviation of uptake and pH over three trials.

electric double layer potential was found by a Laplace solution of the Gouy and Chapman model (eqs S6−S9), which is dependent on the Debye−Huckel double layer length (eq S10) and ionic charge strength of the solution (eq S11). The ionic charge strength was calculated at each pH by summing all positive and negative ion concentrations, including cationic Rh species, anionic Rh species, [H+], and [OH−] present in the liquid solution. Oxide-specific PZNCs were used to calculate the equilibrium of the surface charge density, although the surface charge of the oxide is assumed to be homogeneous across the support. After assigning support-specific parameters, solving for the surface potential as a function of the surface charge density (eqs S12−S14) dictates the surface attraction to oppositely charged ions from solution. The parameters used in the modeling are listed in Table S1.

Figure 2 shows the simulated uptake of Rh ions ($Rh\text{-}(Cl)_x(H_2O)_y(OH)_z^{-2}$ below PZNC and $Rh\text{-}(Cl)_x(H_2O)_y(NH3)_z^{2+}$ above PZNC) modeled for CeO_2 and γ-Al_2O_3 in blue and red solid lines, respectively. The ionic radius of the Rh anion and cation used for the model was estimated based on Rh ion models from literature.[30] As inferred from the PZNC, CeO_2 is predicted to adsorb cationic Rh over a large range above a pH of 8, while anions are predicted to absorb over a narrow range at low pH. Anions are predicted to readily adsorb onto γ-Al_2O_3 below its PZNC and cations above its PZNC.

Figure 2 also shows experimental ICP-OES measurements of the uptake of 200 ppm Rh (nominally 2 wt % Rh) onto (a) CeO_2 and (b) γ-Al_2O_3 as a function of solution pH. A relatively high concentration of Rh was used in these experiments to provide a clear uptake trend, rather than the low Rh concentration that was used to optimize Rh dispersion (discussed below), which often results in 100% uptake. The experimentally measured % Rh uptake onto the oxide supports exhibits similarities and differences compared to the RPA model predictions. On CeO_2, the maximum Rh uptake occurred at pH = 9, while on Al_2O_3, the maximum uptake was observed at pH = 10. At these pHs, the cationic Rh species are the dominant ions in solution, and the RPA model predicts that cations should adsorb on the negatively charged oxide surfaces.[26] The Rh uptake at acidic pH (<7) was higher on γ-Al_2O_3 compared to that on CeO_2. This is consistent with the higher PZNC of γ-Al_2O_3, which creates a stronger driving force for the uptake of anionic Rh species onto the positively charged oxide surface. Uptake of cations in both oxide support cases was best modeled when accounting for the relative cation and anion concentrations measured by ESI-MS because the analysis of speciation accounted for the effect of pH on the ion formation and availability. The experimental uptake near the PZNCs, 7.2 for γ-Al_2O_3 and 3.3 for CeO_2, was likely due to the nonhomogeneous nature of oxide support surfaces, such that there was a mix of negatively and positively charged surface sites for Rh ions to adsorb and was not accounted for in the model.[79−81] Additionally, in contrast to the model, poor experimental Rh uptake at high pH values, 11−12, may be due to oxide dissolution in high concentrations of NH_4OH.[79,82]

3.3. Cryogenic IR and STEM Analysis of Synthesized Materials. Having characterized the adsorption of Rh ions onto the oxide supports, we next used CO probe molecule IR to characterize the structures of Rh formed on the oxide supports as a function of synthesis pH. We hypothesized that conditions that yielded optimum SEA-based Rh uptake would be optimal for forming atomically dispersed Rh species in a modified SEA synthesis procedure. To target the formation of atomically dispersed Rh species, a modified SEA synthesis was performed by slowly injecting a low weight loading of 0.25% Rh in dilute pH-adjusted volumes into the pH-adjusted oxide support solution in an evaporation dish while mixing at a high rate. The water was then slowly evaporated off (for approximately 2.5 h), providing sufficient time for electrostatic adsorption, followed by calcination (at 350 °C in dry air) and then mild reduction (at 200 °C in 10% H_2/Ar). This procedure allows for spatial separation of deposited Rh precursors and minimal mobility of Rh species.[18,22,25,27] The drying step was used, as compared to a traditional filtration step in SEA, such that Rh weight loading could be kept constant at all synthesis pHs and the role of electrostatic adsorption in the formation of atomically dispersed Rh could be independently assessed.

CO probe molecule FTIR analysis was used to assess the Rh structure because it provides unique spectral signatures of bound CO, which correspond to specific structures of Rh deposited on oxide supports.[42] CO binds to supported Rh species on oxide supports in 2:1, 1:1, or 1:2 CO:Rh stoichiometries depending on the type of binding site and Rh structure.[52,83] CO adsorbed to atomically dispersed Rh anchored on oxide supports is known to form Rh gem dicarbonyl species, $Rh(CO)_2$. The two COs can be identified based on two vibrational CO stretching modes, symmetric and

https://doi.org/10.1021/acs.jpcc.2c05426
J. Phys. Chem. C 2022, 126, 18704−18715

asymmetric vibrations at ~2090 and 2020 cm^{-1}, respectively.[83] CO adsorption on extended Rh surfaces, single crystals or particles on oxide supports, results in the formation of bridge-bound species (1 CO to 2 Rh) and linearly bound species (1 CO to 1 Rh), which can be identified by characteristic stretches at 1800−1950 cm^{-1} and 2045−2070 cm^{-1}, respectively.[84−93]

Probe molecule CO-FTIR spectra collected following exposure of the materials to CO at room temperature showed signatures of only $Rh(CO)_2$ species, suggesting that Rh was atomically dispersed in catalysts synthesized under all explored pHs, Figure S4. However, CO probe molecule FTIR spectra collected after exposure of the materials to CO at cryogenic temperatures (< −120 °C) demonstrated the coexistence of atomically dispersed $Rh(CO)_2$ species and CO bound to Rh clusters and a dependence of the Rh structure on synthesis pH, Figure 3. The difference in spectra collected at cryogenic and

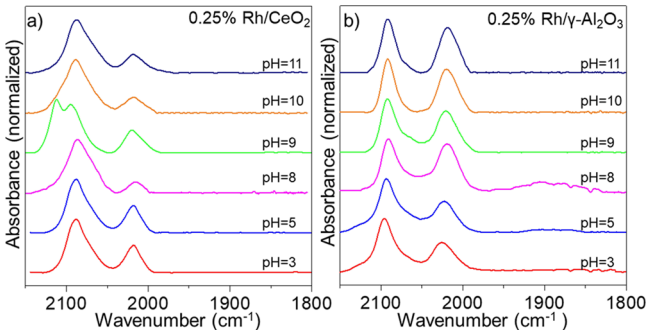

Figure 3. FTIR spectra of CO adsorbed at saturation coverage collected at −120 °C after in situ pretreatment in pure O_2 for 30 min at 350 °C and 10% H_2/Ar for 1 h at 200 °C for (a) 0.25 wt % Rh/CeO_2 and (b) 0.25 wt % Rh/γ-Al_2O_3. Various spectra are shown as a function of the pH of the solution used for Rh deposition onto the oxide. The spectra were normalized to the absorbance of the largest feature in this region and offset for clarity.

room temperature stems from the well-known ability of CO to induce oxidative fragmentation of Rh clusters to form atomically dispersed Rh species.[53,93,94] Performing the measurements at cryogenic temperatures allows the Rh clusters to remain kinetically trapped against fragmentation and effective analysis of the Rh structures in the as-synthesized state. Figure S5 shows CO-FTIR spectra collected at cryogenic temperatures on 1% Rh/CeO_2 that demonstrates the sample initially contained mostly Rh nanoparticles based on the prominent feature at ~2070 cm^{-1}. However, while temperature increased from −120 to 20 °C under vacuum in the 10% CO/Ar flow, the band associated with CO adsorbed to Rh nanoparticles (~2070 cm^{-1}) decreased in intensity while features at ~2090 and 2018 cm^{-1}, associated with $Rh(CO)_2$, increased in intensity, indicating that Rh particle fragmentation into atomically dispersed species occurred. Additionally, it is worth noting that for Rh/CeO_2, room-temperature CO IR shows the formation of carbonates on CeO_2 (likely through CO oxidation), which is largely suppressed by measurements at cryogenic conditions, Figure S6.[95] This is another important distinction based on the temperature of the experiment.

In the cryogenic CO-FTIR measurements in Figure 3a, all Rh/CeO_2 samples showed predominant features at ~2090 and 2018 cm^{-1} associated with atomically dispersed $Rh(CO)_2$ species. The weaker relative intensity of the asymmetric stretch is assigned to electronic asymmetry in the local environment of $Rh(CO)_2$ species, likely caused by a neighboring oxygen vacancy or a reduced Ce metal center.[56] A shoulder at 2070 cm^{-1} on the symmetric $Rh(CO)_2$ vibrational stretch (~2090 cm^{-1}) was observed for all Rh/CeO_2 materials except for at pH = 9 (Figure 3a). In addition, a shoulder appeared at ~2120 cm^{-1} specifically for the pH = 9 synthesis, which has been identified in literature as Rh^{2+} bonded to one CO and an extra O, in addition to the support-derived O.[96,97] This experiment was repeated on multiple samples with consistent results.

Cryogenic CO-FTIR measurements for Rh/γ-Al_2O_3 were generally similar to Rh/CeO_2 with a few differences, Figure 3b. At all synthesis pHs, stretches were predominantly observed at 2091 and 2018 cm^{-1}, associated with $Rh(CO)_2$. Clear signatures of CO bound to Rh clusters or particles were observed at pH < 10 based on measurable absorbance at ~2070 and <1900 cm^{-1}, associated with linearly and bridge-bound CO species, respectively, on Rh clusters or particles. For the synthesis pH of 10 and 11 with γ-Al_2O_3, the $Rh(CO)_2$ spectra still showed a slight deviation from the identical intensity of the two CO stretches expected for a square planar complex. This again suggests a local asymmetry in the environment surrounding $Rh(CO)_2$ at cryogenic temperatures, likely vicinal OH species on the support.[61]

To relate the SEA uptake measurements and model predictions in Figure 2 to the resulting distribution of Rh structures, the fractions of atomically dispersed Rh (X_{iso}) and nanoparticle Rh (X_{nano}) adsorption sites were calculated based on deconvolution analysis of the cryogenic CO-FTIR spectra, Figure S7. X_{iso} and X_{nano} were calculated by deconvoluting the spectra with consistent peak positions and full width at half-maxima (FWHM), shown in Table S2, and using eq S15 with established relative extinction coefficients and adsorption stoichiometries for each vibrational mode.[52,98] Figure S8 provides detailed deconvolution of spectra shown in Figure 3. Table 1 shows the result of this analysis. We note that 0%

Table 1. Fraction of Atomically Dispersed Rh Adsorption Sites (X_{iso}) and Nanoparticle Rh Adsorption Sites (X_{nano}) on 0.25% Rh/CeO_2 and γ-Al_2O_3 at Variable pH

	CeO_2		γ-Al_2O_3	
	0.25 Rh wt %		0.25 Rh wt %	
pH	X_{iso} (%)	X_{nano} (%)	X_{iso} (%)	X_{nano} (%)
3	23	77	26	74
5	22	78	14	86
8	36	64	16	84
9	100	0	40	60
10	43	56	100	0
11	25	75	100	0

site fractions suggest that the contribution of a particular site is below the detection limit. This however does not mean that none of the species exists in the sample; it is simply below detection limits. It is observed that Rh/γ-Al_2O_3 synthesized at pH = 10−11 resulted in the highest fraction of atomically dispersed Rh species, while Rh/CeO_2 samples synthesized at pH = 9 resulted in the highest fraction of atomically dispersed species. Interestingly, the samples with the highest fraction of atomically dispersed Rh species corresponded to synthesis pHs that resulted in the highest Rh uptake in SEA measurements (Figure 2). This provides strong evidence that optimal

https://doi.org/10.1021/acs.jpcc.2c05426
J. Phys. Chem. C 2022, 126, 18704−18715

conditions for SEA-based synthesis (i.e., strong electrostatic interactions between the precursor and support surface) are optimal for the production of atomically dispersed metal catalysts.

To compliment this observation, CO pulse chemisorption measurements performed at 50 °C of the 0.25% Rh/γ-Al_2O_3 material made at pH = 10 have been previously reported by our group with a 2:1 CO:Rh ratio, consistent with ∼100% dispersion of the $Rh(CO)_2$ species.[21] Similar pulse chemisorption measurements are not feasible on the CeO_2 material because CO can be oxidized to form carbonates on CeO_2 at room temperature (as mentioned above), which can result in unreasonable dispersion estimates.[99] While chemisorption measurements at −120 °C would also be useful for comparison to the IR analysis, the low diffusion rate of gases through porous catalyst beds at these temperatures and the large catalyst loadings needed in these measurements washed out the pulsed chemisorption signals.

STEM imaging was used to support the assigned distributions of Rh structures from CO-FTIR measurements. STEM is a common characterization tool to directly demonstrate the existence of atomically dispersed metal species on oxide supports.[41] However, a limited number of localized STEM images may not develop a complete quantitative description of the fraction of atomically dispersed metal species throughout a sample. Thus, coupling STEM with FTIR provides a more insightful confirmation of the distribution of Rh species throughout a given sample. STEM images were collected from samples which showed the highest fraction of atomically dispersed Rh in FTIR measurements, Rh on γ-Al_2O_3 made at pH = 10 (Figure 4a) and Rh on CeO_2 made at pH = 9 (Figure S9), after they had been calcined and reduced ex situ through identical protocols used prior to FTIR characterization.

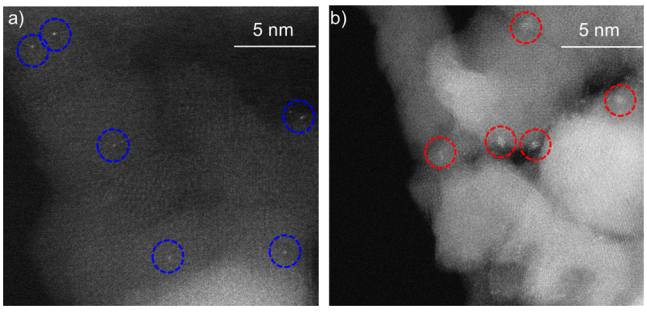

Figure 4. Representative STEM images of samples after pretreatment in pure O_2 for 30 min at 350 °C and 10% H_2/Ar for 1 h at 200 °C for (a) 0.25 wt % Rh/γ-Al_2O_3 made in synthesis solution at pH = 10 and (b) 0.25 wt % Rh/γ-Al_2O_3 made with synthesis solution at pH = 8. Blue circles indicate atomically dispersed Rh species. Red circles indicate Rh clusters.

In Figure 4a, STEM images identified exclusively atomically dispersed Rh species on the 0.25 wt % Rh/γ-Al_2O_3 sample made at pH = 10. Rh is identified in these images as bright spots due to the higher atomic number of Rh (Z = 45) as compared to Al (Z = 13) and the dependence of intensity in HAADF-STEM imaging on Z (intensity $\propto Z^{1.7-2.0}$).[32,100−103] This result agrees with the analysis of IR spectra of the same sample, Figure 3b. It is more challenging to identify atomically dispersed Rh species on CeO_2 through HAADF-STEM imaging because the inherent intensity of Ce atoms, Z = 58, is greater than that of Rh. This was overcome by angling the sample away from the zone axis where Ce ions line up into columns to create contrast for surface-bound Rh atoms.[104] Using this method, STEM images identifying atomically dispersed Rh species on CeO_2 (Figure S9) were acquired, which is again in agreement with the analysis by cryogenic CO probe molecule FTIR, Figure 3a. To contrast the samples where only atomically dispersed species were observed, STEM images were also taken of 0.25 wt % Rh/γ-Al_2O_3 made at pH = 8 (Figure 4b), where a mix of Rh clusters and atomically dispersed species could be identified using cryogenic FTIR. In this sample, more than 50% of the Rh species identified were in the form of small clusters. The STEM results corroborated the conclusion from cryogenic CO IR analysis and reaffirm the assertion that room-temperature CO-FTIR observations do not accurately portray the distribution of Rh structures prior to probe molecule exposure.

While the primary focus here was to identify the role of SEA synthesis in the production of atomically dispersed Rh catalysts at low Rh loadings, it is worth considering how performing synthesis at optimum pH and increasing Rh loadings influence the distribution of Rh structures. Materials were synthesized at support-dependent optimal pH (pH = 9 for CeO_2 and pH = 10 for γ-Al_2O_3) and varying Rh loadings, followed by characterization using cryogenic CO-FTIR. The percentage of atomically dispersed Rh species was quantified, as listed in Table 2,

Table 2. Fraction of Atomically Dispersed Rh Adsorption Sites (X_{iso}) vs Fraction of Nanoparticle Rh Adsorption Sites (X_{nano}) on Rh/CeO_2 and γ-Al_2O_3 at Optimum pH and Variable Rh Weight Loading

	CeO_2 (pH = 9)		γ-Al_2O_3 (pH = 10)	
wt %	X_{iso} (%)	X_{nano} (%)	X_{iso} (%)	X_{nano} (%)
0.1	100	0	100	0
0.25	100	0	100	0
0.5	46	54	100	0
1	22	78	29	71

by calculating the site fraction, eq S15, using site-specific extinction coefficients for adsorbed CO species and accounting for adsorption stoichiometry (ratio of Rh to CO). The relative quantity of atomically dispersed species was estimated by deconvoluting spectra taken at cryogenic temperature and integrating the peak areas associated with CO on various adsorption sites.[52,84,86,93] Again, an entry of 0% simply means that the species is below detection limits. While evidence of CO adsorption on Rh clusters becomes apparent at 0.5 wt % Rh/CeO_2, evidence of CO adsorption on Rh clusters was not prevalent until 1.0 wt % Rh/γ-Al_2O_3 (Figures 5 and S10). Given the surface area of γ-Al_2O_3 being ∼2× larger than CeO_2 used in these studies, the results suggest that the two supports have a similar capacity for supporting atomically dispersed Rh species. We note however that the mobility of Rh species is likely different on the two supports, and thus, higher temperature reductive treatments may produce different structural distributions at the same Rh loading per surface area due to support-dependent Rh mobility.

4. DISCUSSION

The objective of this work was to understand how SEA-based synthesis conditions controlled the resulting distribution of Rh structures on oxide supports. We demonstrated the existence

https://doi.org/10.1021/acs.jpcc.2c05426
J. Phys. Chem. C 2022, 126, 18704−18715

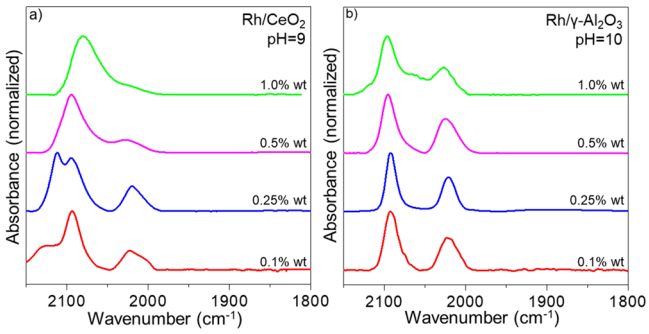

Figure 5. Influence of Rh weight loading on dispersion at optimum synthesis pH. FTIR spectra of CO adsorbed at saturation coverage at −120 °C on materials synthesized at optimized pH and varied Rh weight loading after in situ pretreatment in pure O_2 for 30 min at 350 °C and 10% H_2/Ar for 1 h at 200 °C. (a) Rh/CeO_2 made at pH 9 and (b) Rh/γ-Al_2O_3 made at pH 10. The spectra were normalized to the absorbance of the largest feature in this region and offset for clarity.

of evident trends that relate the uptake of ionic Rh complexes onto CeO_2 and Al_2O_3 as a function of synthesis solution pH to the resulting dispersion of Rh. The relationship between optimal pH for the electrostatic adsorption of Rh and fraction of Rh_{iso} was demonstrated to be consistent with principles of the SEA synthesis technique. The concept of the SEA approach is that the simplest and most effective way to synthesize highly dispersed metal catalysts is to achieve a high dispersion of the metal precursors on the support surface during precursor impregnation. Once impregnated, pretreatment (calcination and reduction) should be done at mild conditions to maintain high metal dispersion.[22,26,27,105] In agreement with SEA principles, pH-controlled solutions promoted repulsive interactions between Rh ions and attractive interactions between the ions and the high-surface-area oxide.[22,26] By modifying the support surface through pH adjustment by the addition of NH_4OH, the oxide surface formed adsorption sites that Coulombically attracted metal ions.[18] The surface potential ultimately dictates the surface attraction to oppositely charged ions and spatially disperses the ions away from sites of the same charge. However, the lack of hydroxyl charge uniformity on the oxide support surface also contributes to uptake seen near the PZNC. Catalysts with lower dispersions were observed in the synthesis pH range between the support PZNC and the point where Rh ionic complexes transition or speciate from anionic to cationic.[64,65,106,107] This suggests that in this pH range, both anionic and cationic Rh species adsorb to positively and negatively charged surface sites and that this may cause Rh adsorption in closer proximity, resulting in facile Rh cluster formation.[52] Further work to optimize the procedure to synthesize atomically dispersed Rh catalysts could provide more detailed modeling of the oxide surface, containing a mix of negatively and positively charged sites.

It is also worth discussing the specific case of Rh deposited on CeO_2 at a pH of 9 in Figures 3 and S7, where an additional CO stretching feature at 2112 cm^{-1} was evident, which has been assigned previously as a single CO bound to an atomically dispersed Rh^{2+} site with an extra O present.[87,93,108] This feature was not observed in spectra collected at room temperature, presumably because the remaining labile O species is reduced by CO to form CO_2. The retained existence of this oxidized Rh species exclusively in the pH of 9 synthesis suggests that Rh was deposited and strongly adsorbed to distinct sites on the CeO_2 support. The potential for site-specific deposition of atomically dispersed metal species on certain supports is an appealing concept to produce active sites with uniform coordination environments.

Another notable difference in the room-temperature CO-FTIR measurement compared to that in the cryogenic measurement was that the asymmetric $Rh(CO)_2$ peak grew in strength with increasing temperature. Figure S11 shows spectra taken, while CO was flown in vacuum as the temperature increased from −120 to 20 °C. This peak ratio has sometimes been connected to the angle between the two CO molecules bonded to Rh.[41,93,109,110] However, recent studies that compare $Rh(CO)_2$ asymmetric to symmetric peak ratios of atomically dispersed Rh on anatase phase TiO_2 to rutile phase TiO_2 have found that the apparent difference in this ratio can also be attributed to nonisotropic electronic interactions between $Rh(CO)_2$ and surface oxygen vacancies in rutile TiO_2. Thus, saying that the asymmetric to symmetric peak ratio changes due to bond angle is a simplification that requires further research for a complete explanation. This change in spectral shape as a function of temperature does however show the importance of using cryogenic CO-FTIR measurements to characterize the Rh coordination environment prior to being influenced by CO adsorption. Thus, cryogenic analysis CO-FTIR is an important tool for characterizing the structure and local environment of atomically dispersed Rh species because CO exposure at room temperature can cause Rh cluster fragmentation, reconstruction of the $Rh(CO)_2$ species, and reactions with species adsorbed to Rh.

5. CONCLUSIONS

By examining the effect of solution pH during SEA-based catalyst synthesis on support surface charge and Rh precursor speciation, we identified the optimal conditions for ionic Rh species to disperse on oxide supports. Via a combination of SEA-based Rh deposition at varying pH, cryogenic CO-FTIR spectroscopy, and HAADF-STEM imaging, it was demonstrated that the optimum conditions for SEA-based Rh deposition correlated with the optimal conditions for forming atomically dispersed Rh species. For the synthesis of atomically dispersed Rh species from $RhCl_3$ precursors, optimum deposition pHs of 9 and 10−11 were identified for CeO_2 and γ-Al_2O_3, respectively. Furthermore, it was demonstrated that it is critical to utilize cryogenic CO-FTIR measurements, as compared to room-temperature measurements, to characterize the structure and coordination environment of the synthesized Rh species. The synthesis and characterization tools reported here could be important for the development of structure−function relationships in supported Rh catalysts.

■ ASSOCIATED CONTENT

Supporting Information

The Supporting Information is available free of charge at https://pubs.acs.org/doi/10.1021/acs.jpcc.2c05426.

PZNC evaluation, Rh ion ESI-MS, RPA model equations and variables, room-temperature CO probe molecule FTIR, Rh nanoparticles on ceria: CO probe molecule FTIR from cryogenic to room temperature, carbonate formation on Rh/CeO_2 at room temperature during CO exposure, method for quantifying site fractions, HAADF-STEM atomically dispersed Rh on

https://doi.org/10.1021/acs.jpcc.2c05426
J. Phys. Chem. C 2022, 126, 18704−18715

ceria, deconvolution of CO IR spectra at optimum pH and varied weight loading, and atomically dispersed Rh on ceria CO probe molecule FTIR from cryogenic to room temperature. (PDF)

AUTHOR INFORMATION

Corresponding Author

Phillip Christopher − *Department of Chemical Engineering, University of California Santa Barbara, Santa Barbara, California 93106, United States;* orcid.org/0000-0002-4898-5510; Email: pchristopher@ucsb.edu

Authors

Chithra Asokan − *Department of Chemical Engineering, University of California Santa Barbara, Santa Barbara, California 93106, United States*

Mingjie Xu − *Department of Materials Science and Engineering, University of California Irvine, Irvine, California 92697, United States*

Sheng Dai − *Department of Materials Science and Engineering, University of California Irvine, Irvine, California 92697, United States;* orcid.org/0000-0001-5787-0179

Xiaoqing Pan − *Department of Materials Science and Engineering, Department of Physics and Astronomy, and Irvine Materials Research Institute (IMRI), University of California Irvine, Irvine, California 92697, United States*

Complete contact information is available at: https://pubs.acs.org/10.1021/acs.jpcc.2c05426

Notes

The authors declare no competing financial interest.

ACKNOWLEDGMENTS

This work was supported by the National Science Foundation (NSF) GOALI Grant CBET-1804128 and Mellichamp Initiative for Sustainability at the University of California, Santa Barbara. The UCSB MRL Facility is acknowledged for the use of shared ICP-OES supported by the MRSEC Program of the National Science Foundation under award no. DMR 1720256. Dr. Dmitriy Uchenik from the UCSB Mass Spectroscopy Facility is acknowledged for assistance with ESI-MS measurements. The authors acknowledge the use of facilities and instrumentation at the UC Irvine Materials Research Institute (IMRI) supported in part by the NSF through the MRSEC program (DMR-2011967).

REFERENCES

(1) Armor, J. N. A History of Industrial Catalysis. *Catal. Today* **2011**, *163*, 3−9.

(2) Shelef, M.; Graham, G. W. Why Rhodium in Automotive Three-Way Catalysts? *Catal. Rev.* **1994**, *36*, 433−457.

(3) Shelef, M.; McCabe, R. W. Twenty-Five Years after Introduction of Automotive Catalysts: What Next? *Catal. Today* **2000**, *62*, 35−50.

(4) Collins, N. R.; Twigg, M. V. Three-Way Catalyst Emissions Control Technologies for Spark-Ignition Engines—Recent Trends and Future Developments. *Top. Catal.* **2007**, *42-43*, 323−332.

(5) Asokan, C.; Yang, Y.; Dang, A.; Getsoian, A.; Christopher, P. Low-Temperature Ammonia Production during NO Reduction by CO Is Due to Atomically Dispersed Rhodium Active Sites. *ACS Catal.* **2020**, *10*, 5217−5222.

(6) Lou, Y.; Liu, J. CO Oxidation on Metal Oxide Supported Single Pt Atoms: The Role of the Support. *Ind. Eng. Chem. Res.* **2017**, *56*, 6916−6925.

(7) Haruta, M. Size- and Support-Dependency in the Catalysis of Gold. *Catal. Today* **1997**, *36*, 153−166.

(8) Andersson, M. P.; Abild-Pedersen, F.; Remediakis, I. N.; Bligaard, T.; Jones, G.; Engbæk, J.; Lytken, O.; Horch, S.; Nielsen, J. H.; Sehested, J.; Nørskov, J. K.; Chorkendorff, I. Structure Sensitivity of the Methanation Reaction: H2-Induced CO Dissociation on Nickel Surfaces. *J. Catal.* **2008**, *255*, 6−19.

(9) Hammer, B. Special Sites at Noble and Late Transition Metal Catalysts. *Top. Catal.* **2006**, *37*, 3−16.

(10) Haruta, M. When Gold Is Not Noble: Catalysis by Nanoparticles. *Chem. Rec.* **2003**, *3*, 75−87.

(11) Liu, J.; Chen, J.; Liu, P.; Zhang, H.; Li, G.; An, T.; Zhao, H. Catalysis by Supported Single Metal Atoms. *ACS Catal.* **2016**, 34−41.

(12) Yang, X.; Wang, A.; Qiao, B.; Li, J. U. N.; Liu, J.; Zhang, T. Single-Atom Catalysts: A New Frontier in Heterogeneous Catalysis. *Acc. Chem. Res.* **2013**, *46*, 1740−1748.

(13) Qi, J.; Christopher, P. Atomically Dispersed Rh Active Sites on Oxide Supports with Controlled Acidity for Gas-Phase Halide-Free Methanol Carbonylation to Acetic Acid. *Ind. Eng. Chem. Res.* **2019**, *58*, 12632−12641.

(14) Nørskov, J. K.; Bligaard, T.; Hvolbæk, B.; Abild-Pedersen, F.; Chorkendorff, I.; Christensen, C. H. The Nature of the Active Site in Heterogeneous Metal Catalysis. *Chem. Soc. Rev.* **2008**, *37*, 2163−2171.

(15) Ji, S.; Chen, Y.; Wang, X.; Zhang, Z.; Wang, D.; Li, Y. Chemical Synthesis of Single Atomic Site Catalysts. *Chem. Rev.* **2020**, *120*, 11900−11955.

(16) Karelovic, A.; Ruiz, P. Mechanistic Study of Low Temperature CO_2 Methanation over Rh/TiO_2 Catalysts. *J. Catal.* **2013**, *301*, 141−153.

(17) Panagiotopoulou, P.; Kondarides, D. I.; Verykios, X. E. Selective Methanation of CO over Supported Noble Metal Catalysts: Effects of the Nature of the Metallic Phase on Catalytic Performance. *Appl. Catal. A Gen.* **2008**, *344*, 45−54.

(18) DeRita, L.; Dai, S.; Lopez-Zepeda, K.; Pham, N.; Graham, G. W.; Pan, X.; Christopher, P. Catalyst Architecture for Stable Single Atom Dispersion Enables Site-Specific Spectroscopic and Reactivity Measurements of CO Adsorbed to Pt Atoms, Oxidized Pt Clusters, and Metallic Pt Clusters on TiO2. *J. Am. Chem. Soc.* **2017**, *139*, 14150−14165.

(19) Resasco, J.; DeRita, L.; Dai, S.; Chada, J. P.; Xu, M.; Yan, X.; Finzel, J.; Hanukovich, S.; Hoffman, A. S.; Graham, G. W.; Bare, S. R.; Pan, X.; Christopher, P. Uniformity Is Key in Defining Structure−Function Relationships for Atomically Dispersed Metal Catalysts: The Case of Pt/CeO2. *J. Am. Chem. Soc.* **2020**, *142*, 169−184.

(20) DeRita, L.; Resasco, J.; Dai, S.; Boubnov, A.; Thang, H. V.; Hoffman, A. S.; Ro, I.; Graham, G. W.; Bare, S. R.; Pacchioni, G.; et al. Structural Evolution of Atomically Dispersed Pt Catalysts Dictates Reactivity. *Nat. Mater.* **2019**, *18*, 746−751.

(21) Zakem, G.; Ro, I.; Finzel, J.; Christopher, P. Support Functionalization as an Approach for Modifying Activation Entropies of Catalytic Reactions on Atomically Dispersed Metal Sites. *J. Catal.* **2021**, *404*, 883−896.

(22) Jiao, L.; Regalbuto, J. R. The Synthesis of Highly Dispersed Noble and Base Metals on Silica via Strong Electrostatic Adsorption: II. Mesoporous Silica SBA-15. *J. Catal.* **2008**, *260*, 342−350.

(23) Schreier, M.; Regalbuto, J. R. A Fundamental Study of Pt Tetraammine Impregnation of Silica: 1. The Electrostatic Nature of Platinum Adsorption. *J. Catal.* **2004**, *225*, 190−202.

(24) Park, J.; Regalbuto, J. R. A Simple, Accurate Determination of Oxide PZC and the Strong Buffering Effect of Oxide Surfaces at Incipient Wetness. *J. Colloid Interface Sci.* **1995**, *175*, 239−252.

(25) Miller, J. T.; Schreier, M.; Kropf, A. J.; Regalbuto, J. R. A Fundamental Study of Platinum Tetraammine Impregnation of Silica: 2. The Effect of Method of Preparation, Loading, and Calcination Temperature on (Reduced) Particle Size. *J. Catal.* **2004**, *225*, 203−212.

(26) Regalbuto, J. R. A Scientific Method to Prepare Supported Metal Catalysts. In *Surface and nanomolecular catalysis*; CRC Press, 2006; 175−208.
(27) Regalbuto, J. R. A Simple, Rational Method to Prepare Nanodispersed Metal Catalysts Supported on Silica. In *Silica and Silicates in Modern Catalysis*; Transworld Research Network, 2010; *42*, 345−374.
(28) Uheida, A.; Iglesias, M.; Fontàs, C.; Hidalgo, M.; Salvadó, V.; Zhang, Y.; Muhammed, M. Sorption of Palladium(II), Rhodium(III), and Platinum(IV) on Fe3O4 Nanoparticles. *J. Colloid Interface Sci.* **2006**, *301*, 402−408.
(29) Martens, J. H. A.; Prins, R. Influence of PH on the Preparation of Monometallic Rhodium and Platinum, and Bimetallic Rhodium Platinum Catalysts Supported on γ-Alumina. *Appl. Catal.* **1989**, *46*, 31−44.
(30) Yusenko, K. V.; Sukhikh, A. S.; Kraus, W.; Gromilov, S. A. Synthesis and Crystal Chemistry of Octahedral Rhodium (III) Chloroamines. *Molecules* **2020**, *25*, 768.
(31) Palmer, D. A.; Harris, G. M. Kinetics, Mechanism, and Stereochemistry of the Aquation and Chloride Anation Reactions of Fac- and Mer-Trichlorotriaquorhodium(III) Complexes in Acidic Aqueous Solution. A Complete Reaction Scheme for Complex Ions of the General Formula [RhCln(OH2)6-n] 3. *Inorg. Chem.* **1975**, *14*, 1316−1321.
(32) Ro, I.; Xu, M.; Graham, G. W.; Pan, X.; Christopher, P. Synthesis of Heteroatom Rh−ReOx Atomically Dispersed Species on Al2O3 and Their Tunable Catalytic Reactivity in Ethylene Hydroformylation. *ACS Catal.* **2019**, *9*, 10899−10912.
(33) Keels, J. M.; Chen, X.; Karakalos, S.; Liang, C.; Monnier, J. R.; Regalbuto, J. R. Aqueous-Phase Hydrogenation of Succinic Acid Using Bimetallic Ir − Re/C Catalysts Prepared by Strong Electrostatic Adsorption. *ACS Catal.* **2018**, *8*, 6486−6494.
(34) Hao, X.; Barnes, S.; Regalbuto, J. R. A Fundamental Study of Pt Impregnation of Carbon: Adsorption Equilibrium and Particle Synthesis. *J. Catal.* **2011**, *279*, 48−65.
(35) Feltes, T. E.; Espinosa-Alonso, L.; de Smit, E.; D'Souza, L.; Meyer, R. J.; Weckhuysen, B. M.; Regalbuto, J. R. Selective Adsorption of Manganese onto Cobalt for Optimized Mn/Co/TiO2 Fischer−Tropsch Catalysts. *J. Catal.* **2010**, *270*, 95−102.
(36) Zhu, X.; Cho, H.; Pasupong, M.; Regalbuto, J. R. Charge-Enhanced Dry Impregnation A Simple Way to Improve the Preparation of Supported Metal Catalysts. *ACS Catal.* **2013**, *3*, 625−630.
(37) Onn, T. M.; Zhang, S.; Arroyo-Ramirez, L.; Xia, Y.; Wang, C.; Pan, X.; Graham, G. W.; Gorte, R. J. High-Surface-Area Ceria Prepared by ALD on Al2O3 Support. *Appl. Catal. B* **2017**, *201*, 430−437.
(38) Resasco, J.; Dai, S.; Graham, G.; Pan, X.; Christopher, P. Combining In-Situ Transmission Electron Microscopy and Infrared Spectroscopy for Understanding Dynamic and Atomic-Scale Features of Supported Metal Catalysts. *J. Phys. Chem. C* **2018**, *122*, 25143−25157.
(39) Badwal, S. P. S.; Fini, D.; Ciacchi, F. T.; Munnings, C.; Kimpton, J. A.; Drennan, J. Structural and Microstructural Stability of Ceria − Gadolinia Electrolyte Exposed to Reducing Environments of High Temperature Fuel Cells. *J. Mater. Chem. A Mater.* **2013**, *1*, 10768−10782.
(40) Ryczkowski, J. IR Spectroscopy in Catalysis. *Catal. Today* **2001**, *68*, 263−381.
(41) Asokan, C.; Derita, L.; Christopher, P. Using Probe Molecule FTIR Spectroscopy to Identify and Characterize Pt - Group Metal Based Single Atom Catalysts. *Chin. J. Catal.* **2017**, *38*, 1473−1480.
(42) Lamberti, C.; Zecchina, A.; Groppo, E.; Bordiga, S. Probing the Surfaces of Heterogeneous Catalysts by in Situ IR Spectroscopy. *Chem. Soc. Rev.* **2010**, *39*, 4951−5001.
(43) Chakarova, K.; Mihaylov, M.; Hadjiivanov, K. FTIR Spectroscopic Study of CO Adsorption on Pt − H − ZSM-5. *Microporous Mesoporous Mater.* **2005**, *81*, 305−312.
(44) Stakheev, A. Y.; Shpiro, E. S.; Tkachenko, O. P.; Jaeger, N. I.; Schulz-Ekloff, G. Evidence for Monatomic Platinum Species in H-ZSM-5 from FTIR Spectroscopy of Chemisorbed CO. *J. Catal.* **1997**, *169*, 382−388.
(45) Khivantsev, K.; Vityuk, A.; Aleksandrov, H. A.; Vayssilov, G. N.; Blom, D.; Alexeev, O. S.; Amiridis, M. D. Synthesis, Modelling, and Catalytic Properties of HY Zeolite- Supported Rhodium Dinitrosyl Complexes. *ACS Catal.* **2017**, *7*, 5965−5982.
(46) Hoffman, A. S.; Fang, C. Y.; Gates, B. C. Homogeneity of Surface Sites in Supported Single-Site Metal Catalysts: Assessment with Band Widths of Metal Carbonyl Infrared Spectra. *J. Phys. Chem. Lett.* **2016**, *7*, 3854−3860.
(47) Zhang, B.; Asakura, H.; Yan, N. Atomically Dispersed Rhodium on Self-Assembled Phosphotungstic Acid: Structural Features and Catalytic CO Oxidation Properties. *Ind. Eng. Chem. Res.* **2017**, *56*, 3578−3587.
(48) Peterson, E. J.; DeLaRiva, A. T.; Lin, S.; Johnson, R. S.; Guo, H.; Miller, J. T.; Hun Kwak, J.; Peden, C. H. F.; Kiefer, B.; Allard, L. F.; et al. Low-Temperature Carbon Monoxide Oxidation Catalysed by Regenerable Atomically Dispersed Palladium on Alumina. *Nat. Commun.* **2014**, *5*, 4885.
(49) Guzman, J.; Gates, B. C. Supported Molecular Catalysts: Metal Complexes and Clusters on Oxides and Zeolites. *Dalton Trans.* **2003**, *17*, 3303−3318.
(50) Hyde, E. A.; Robert, R.; Rochester, C. H. Infrared Study of the Interactions between NO and CO on Rh / Al2O3 Catalysts. *J. Chem. Soc., Faraday Trans. 1* **1984**, *80*, 531−541.
(51) Granger, P.; Delannoy, L.; Lecomte, J. J.; Dathy, C.; Praliaud, H.; Leclercq, L.; Leclercq, G. Kinetics of the CO + NO Reaction over Bimetallic Platinum-Rhodium on Alumina: Effect of Ceria Incorporation into Noble Metals. *J. Catal.* **2002**, *207*, 202−212.
(52) Matsubu, J. C.; Yang, V. N.; Christopher, P. Isolated Metal Active Site Concentration and Stability Controls Catalytic CO2 Reduction Selectivity. *J. Am. Chem. Soc.* **2015**, *137*, 3076−3084.
(53) Goldsmith, B. R.; Sanderson, E. D.; Ouyang, R.; Li, W. X. CO- and NO-Induced Disintegration and Redispersion of Three-Way Catalysts Rhodium, Palladium, and Platinum: An Ab Initio Thermodynamics Study. *J. Phys. Chem. C* **2014**, *118*, 9588−9597.
(54) Uzun, A.; Gates, B. C. Real-time Characterization of Formation and Breakup of Iridium Clusters in Highly Dealuminated Zeolite Y. *Angew. Chem., Int. Ed.* **2008**, *47*, 9245−9248.
(55) Uzun, A.; Gates, B. C. Dynamic Structural Changes in a Molecular Zeolite-Supported Iridium Catalyst for Ethene Hydrogenation. *J. Am. Chem. Soc.* **2009**, *131*, 15887−15894.
(56) Tang, Y.; Asokan, C.; Xu, M.; Graham, G. W.; Pan, X.; Christopher, P.; Li, J.; Sautet, P. Rh Single Atoms on TiO2 Dynamically Respond to Reaction Conditions by Adapting Their Site. *Nat. Commun.* **2019**, *10*, 4488.
(57) Hoffman, A. J.; Asokan, C.; Gadinas, N.; Schroeder, E.; Zakem, G.; Nystrom, S. V.; Getsoian, A.; Christopher, P.; Hibbitts, D. Experimental and Theoretical Characterization of Rh Single Atoms Supported on γ-Al2O3 with Varying Hydroxyl Contents during NO Reduction by CO. *ACS Catal.* **2022**, 11697−11715.
(58) Qiao, B.; Wang, A.; Yang, X.; Allard, L. F.; Jiang, Z.; Cui, Y.; Liu, J.; Li, J.; Zhang, T. Single-Atom Catalysis of CO Oxidation Using Pt1/FeOx. *Nat. Chem.* **2011**, *3*, 634−641.
(59) Hadjiivanov, K. Identification and Characterization of Surface Hydroxyl Groups by Infrared Spectroscopy. In *Advances in Catalysis*; Elsevier Inc., 2014, *57*, 99 −318.
(60) Chizallet, C.; Digne, M.; Arrouvel, C.; Raybaud, P.; Delbecq, F.; Costentin, G.; Che, M.; Sautet, P.; Toulhoat, H. Insights into the Geometry, Stability and Vibrational Properties of OH Groups on γ-Al2O3, TiO2-Anatase and MgO from DFT Calculations. *Top. Catal.* **2009**, *52*, 1005−1016.
(61) Asokan, C.; Thang, H. V.; Pacchioni, G.; Christopher, P. Reductant Composition Influences the Coordination of Atomically Dispersed Rh on Anatase TiO2. *Catal. Sci. Technol.* **2020**, *10*, 1597−1601.

https://doi.org/10.1021/acs.jpcc.2c05426
J. Phys. Chem. C 2022, 126, 18704−18715

(62) Hao, X.; Quach, L.; Korah, J.; Spieker, W. A.; Regalbuto, J. R. The Control of Platinum Impregnation by PZC Alteration of Oxides and Carbon. *J. Mol. Catal. A: Chem.* **2004**, *219*, 97−107.
(63) Trueba, M.; Trasatti, S. P. Γ-Alumina as a Support for Catalysts: A Review of Fundamental Aspects. *Eur. J. Inorg. Chem.* **2005**, *2005*, 3393−3403.
(64) Colombo, C.; Oates, C. J.; Monhemius, A. J.; Plant, J. A. Complexation of Platinum, Palladium and Rhodium with Inorganic Ligands in the Environment. *Geochem.: Explor., Environ., Anal.* **2008**, *8*, 91−101.
(65) Benguerel, E.; Demopoulos, G. P.; Harris, G. B. Speciation and Separation of Rhodium (III) from Chloride Solutions: A Critical Review. *Hydrometallurgy* **1996**, *40*, 135−152.
(66) Wolsey, B. W. C.; Reynolds, C. A.; Kleinberg, J. Complexes in the Rhodium (III) -Chloride System in Acid Solution. *Inorg. Chem.* **1963**, *2*, 463−468.
(67) Gerber, W. J.; Koch, K. R.; Rohwer, H. E.; Hosten, E. C.; Geswindt, T. E. Separation and Quantification of [RhCln (H2O) 6− n] 3− n (N= 0−6) Complexes, Including Stereoisomers, by Means of Ion-Pair HPLC−ICP-MS. *Talanta* **2010**, *82*, 348−358.
(68) Endo, K.; Saikawa, M.; Sugimoto, M.; Hada, M.; Nakatsuji, H. Theoretical Study of the Transition Energies of the Visible Absorption Spectra of [RhCl6] 3− and [RhCl5 (H2O)] 2− Complexes in Aqueous Solution. *Bull. Chem. Soc. Jpn.* **1995**, *68*, 1601−1605.
(69) Samuels, A. C.; Boele, C. A.; Bennett, K. T.; Clark, S. B.; Wall, N. A.; Clark, A. E. Integrated Computational and Experimental Protocol for Understanding Rh (III) Speciation in Hydrochloric and Nitric Acid Solutions. *Inorg. Chem.* **2014**, *53*, 12315−12322.
(70) Vasilchenko, D. B.; Berdyugin, S. N.; Korenev, S. V.; O'Kennedy, S.; Gerber, W. J. Spectroscopic and DFT Study of RhIII Chloro Complex Transformation in Alkaline Solutions. *Inorg. Chem.* **2017**, *56*, 10724−10734.
(71) Le, M. N.; Lee, M. S.; Senanayake, G. A Short Review of the Separation of Iridium and Rhodium from Hydrochloric Acid Solutions by Solvent Extraction. *J. Solution Chem.* **2018**, *47*, 1373−1394.
(72) Nadolinny, V.; Belyaev, A.; Komarovskikh, A.; Tkachev, S.; Yushina, I. The Photochemical Generation of Superoxide Rh (Iii) Complexes. *New J. Chem.* **2018**, *42*, 15231−15236.
(73) Mahlamvana, F.; Kriek, R. J. Photocatalytic Reduction of [RhCln (H2O) 6− n] 3− n (N= 0−6) in a Titanium Dioxide Suspension: The Role of Structurally Different Sacrificial Reducing Agents. *Appl. Catal. B* **2015**, *162*, 445−453.
(74) McSkimming, A.; Bhadbhade, M.; Colbran, S. B. Hydride Ion-Carrier Ability in Rh (I) Complexes of a Nicotinamide-Functionalised N-Heterocyclic Carbene Ligand. *Dalton Trans.* **2010**, *39*, 10581−10584.
(75) Ho, C. S.; Lam, C. W. K.; Chan, M. H. M.; Cheung, R. C. K.; Law, L. K.; Lit, L. C. W.; Ng, K. F.; Suen, M. W. M.; Tai, H. Electrospray Ionisation Mass Spectrometry: Principles and Clinical Applications. *Clin. Biochem. Rev.* **2003**, *24*, 3−12.
(76) Sánchez, J. M.; Hidalgo, M.; Havel, J.; Salvadó, V. The Speciation of Rhodium (III) in Hydrochloric Acid Media by Capillary Zone Electrophoresis. *Talanta* **2002**, *56*, 1061−1071.
(77) Robb, W.; Harris, G. M. Some Exchange and Substitution Reactions of Ions in Aqueous Acid Solutions. *J. Am. Chem. Soc.* **1965**, *87*, 4472−4476.
(78) Robb, W.; Steyn, V. Kinetics of Aquation of Aquopentachlororhodium (III) and Chloride Anation of Diaquotetrachlororhodium (III) Anions. *Inorg. Chem.* **1966**, *6*, 616−619.
(79) Rudziński, W.; Piasecki, W.; Janusz, W.; Panas, G.; Charmas, R. A Thermodynamic Analysis of Ion Adsorption in the Metal Oxide/Electrolyte Systems in Which PZC and CIP Do Not Coincide. *Adsorption* **2001**, *7*, 327−338.
(80) Panagiotou, G. D.; Petsi, T.; Bourikas, K.; Garoufalis, C. S.; Tsevis, A.; Spanos, N.; Kordulis, C.; Lycourghiotis, A. Mapping the Surface (Hydr) Oxo-Groups of Titanium Oxide and Its Interface with an Aqueous Solution: The State of the Art and a New Approach. *Adv. Colloid Interface Sci.* **2008**, *142*, 20−42.
(81) Busca, G. The Surface of Transitional Aluminas: A Critical Review. *Catal. Today* **2014**, *226*, 2−13.
(82) Franks, G. V.; Gan, Y. Charging Behavior at the Alumina−Water Interface and Implications for Ceramic Processing. *J. Am. Ceram. Soc.* **2007**, *90*, 3373−3388.
(83) Yang, C.; Garland, C. W. Infrared Studies of Carbon Monoxide Chemisorbed on Rhodium. *J. Phys. Chem.* **1957**, *61*, 1504−1512.
(84) Duncan, T. M.; Vaughan, R. W. A 13C NMR Study of the Adsorbed States of CO on Rh Dispersed on Al2O3. *J. Chem. Phys.* **1980**, *73*, 975−985.
(85) Rice, C. A.; Worley, S. D.; Curtis, C. W.; Guin, J. A.; Tarrer, A. R. The Oxidation State of Dispersed Rh on Al2O3. *J. Chem. Phys.* **1981**, *74*, 6487−6497.
(86) Cavanagh, R. R.; Yates, J. T. Site Distribution Studies of Rh Supported on Al2O3—An Infrared Study of Chemisorbed CO. *J. Chem. Phys.* **1981**, *74*, 4150−4155.
(87) Yates, J. T., Jr.; Kolasinski, K. Infrared Spectroscopic Investigation of the Rhodium Gem-Dicarbonyl Surface Species. *J. Chem. Phys.* **1983**, *79*, 1026−1030.
(88) Solymosi, F.; Pasztor, M. An Infrared Study of the Influence of Carbon Monoxide Chemisorption on the Topology of Supported Rhodium. *J. Phys. Chem.* **1985**, *89*, 4789−4793.
(89) Trautmann, S.; Baerns, M. Infrared Spectroscopic Studies of CO Adsorption on Rhodium Supported by SiO2, Al2O3, and TiO2. *J. Catal.* **1994**, *150*, 335−344.
(90) Goellner, J. F.; Gates, B. C.; Vayssilov, G. N.; Rösch, N. Structure and Bonding of a Site-Isolated Transition Metal Complex: Rhodium Dicarbonyl in Highly Dealuminated Zeolite y. *J. Am. Chem. Soc.* **2000**, *122*, 8056−8066.
(91) Serna, P.; Gates, B. C. Zeolite-Supported Rhodium Complexes and Clusters: Switching Catalytic Selectivity by Controlling Structures of Essentially Molecular Species. *J. Am. Chem. Soc.* **2011**, *133*, 4714−4717.
(92) Hoffman, A. J.; Asokan, C.; Gadinas, N.; Kravchenko, P.; Getsoian, A.; Christopher, P.; Hibbitts, D. Theoretical and Experimental Characterization of Adsorbed CO and NO on γ-Al2O3-Supported Rh Nanoparticles. *J. Phys. Chem. C* **2021**, *125*, 19733−19755.
(93) Yates, J. T., Jr.; Duncan, T. M.; Worley, S. D.; Vaughan, R. W. Infrared Spectra of Chemisorbed CO on Rh. *J. Chem. Phys.* **1979**, *70*, 1219−1224.
(94) Novak, E.; Sprinceana, D.; Solymosi, F. CO-Induced Structural Changes of Supported Rh Promoted by NO. *Appl. Catal. A Gen.* **1997**, *149*, 89−101.
(95) Vayssilov, G. N.; Mihaylov, M.; Petkov, P.; Hadjiivanov, K. I.; Neyman, K. M. Reassignment of the Vibrational Spectra of Carbonates, Formates, and Related Surface Species on Ceria: A Combined Density Functional and Infrared Spectroscopy Investigation. *J. Phys. Chem. C* **2011**, *115*, 23435−23454.
(96) Finocchio, E.; Busca, G.; Forzatti, P.; Groppi, G.; Beretta, A. State of Supported Rhodium Nanoparticles for Methane Catalytic Partial Oxidation (CPO), FT-IR Studies. *Langmuir* **2007**, *23*, 10419−10428.
(97) Kistler, J. D.; Chotigkrai, N.; Xu, P.; Enderle, B.; Praserthdam, P.; Chen, C.; Browning, N. D.; Gates, B. C. A Single-site Platinum CO Oxidation Catalyst in Zeolite KLTL: Microscopic and Spectroscopic Determination of the Locations of the Platinum Atoms. *Angew. Chem., Int. Ed.* **2014**, *53*, 8904−8907.
(98) Resasco, J.; Yang, F.; Mou, T.; Wang, B.; Christopher, P.; Resasco, D. E. Relationship between Atomic Scale Structure and Reactivity of Pt Catalysts: Hydrodeoxygenation of m-Cresol over Isolated Pt Cations and Clusters. *ACS Catal.* **2019**, *10*, 595−603.
(99) Tanabe, T.; Nagai, Y.; Hirabayashi, T.; Takagi, N.; Dohmae, K.; Takahashi, N.; Matsumoto, S.; Shinjoh, H.; Kondo, J. N.; Schouten, J. C.; et al. Low Temperature CO Pulse Adsorption for the Determination of Pt Particle Size in a Pt/Cerium-Based Oxide Catalyst. *Appl. Catal. A Gen.* **2009**, *370*, 108−113.
(100) Ezekoye, O. K.; Drews, A. R.; Jen, H.-W.; Kudla, R. J.; McCabe, R. W.; Sharma, M.; Howe, J. Y.; Allard, L. F.; Graham, G.

https://doi.org/10.1021/acs.jpcc.2c05426
J. Phys. Chem. C 2022, 126, 18704−18715

W.; Pan, X. Q. Characterization of Alumina-Supported Pt and Pt−Pd NO Oxidation Catalysts with Advanced Electron Microscopy. *J. Catal.* **2011**, *280*, 125−136.
(101) Pennycook, S. J. Z-Contrast STEM for Materials Science. *Ultramicroscopy* **1989**, *30*, 58−69.
(102) Pennycook, S. J. Z-Contrast Transmission Electron Microscopy: Direct Atomic Imaging of Materials. *Annu. Rev. Mater. Sci.* **1992**, *22*, 171−195.
(103) Pennycook, S. J.; Nellist, P. D. Z-Contrast Scanning Transmission Electron Microscopy. In *Impact of electron and scanning probe microscopy on materials research*; Springer, 1999; 161−207.
(104) Tieu, P.; Yan, X.; Xu, M.; Christopher, P.; Pan, X. Directly Probing the Local Coordination, Charge State, and Stability of Single Atom Catalysts by Advanced Electron Microscopy: A Review. *Small* **2021**, *17*, No. 2006482.
(105) Regalbuto, J. R.; Navada, A.; Shadid, S.; Bricker, M. L.; Chen, Q. An Experimental Verification of the Physical Nature of Pt Adsorption onto Alumina. *J. Catal.* **1999**, *184*, 335−348.
(106) Svecova, L.; Papaïconomou, N.; Billard, I. Rh (III) Aqueous Speciation with Chloride as a Driver for Its Extraction by Phosphonium Based Ionic Liquids. *Molecules* **2019**, *24*, 1391.
(107) Volchek, V. V.; Berdyugin, S. N.; Shuvaeva, O. V.; Sheven, D. G.; Vasilchenko, D. B.; Korenev, S. V. Rh (III) Hydroxocomplexes Speciation Using HPLC-ESI-MS. *Anal. Methods* **2020**, *12*, 2631−2637.
(108) Basu, P.; Panayotov, D.; Yates, J. T. Rhodium-Carbon Monoxide Surface Chemistry: The Involvement of Surface Hydroxyl Groups on Alumina and Silica Supports. *J. Am. Chem. Soc.* **1988**, *110*, 2074−2081.
(109) Babucci, M.; Hoffman, A. S.; Debefve, L. M.; Kurtoglu, S. F.; Bare, S. R.; Gates, B. C.; Uzun, A. Unraveling the Individual Influences of Supports and Ionic Liquid Coatings on the Catalytic Properties of Supported Iridium Complexes and Iridium Clusters. *J. Catal.* **2020**, *387*, 186−195.
(110) Miessner, H.; Burkhardt, I.; Gutschick, D.; Zecchina, A.; Morterra, C.; Spoto, G. The Formation of a Well Defined Rhodium Dicarbonyl in Highly Dealuminated Rhodium-Exchanged Zeolite Y by Interaction with CO. *J. Chem. Soc., Faraday Trans. 1* **1989**, *85*, 2113−2126.

https://doi.org/10.1021/acs.jpcc.2c05426
J. Phys. Chem. C 2022, 126, 18704−18715